

Driven Dirac-like Equation via Mirror Oscillation: Controlled Cold-Atom Zitterbewegung

Qi Zhang,¹ Jiangbin Gong,^{2,3} and C.H. Oh^{1,4}

¹*Centre of Quantum Technologies and Department of Physics,
National University of Singapore, 117543, Singapore*

²*Department of Physics and Centre for Computational Science and Engineering,
National University of Singapore, 117542, Singapore*

³*NUS Graduate School for Integrative Sciences and Engineering, Singapore 117597, Republic of Singapore*

⁴*Institute of Advanced Studies, Nanyang Technological University, Singapore 639798, Republic of Singapore*
(Dated: November 14, 2018)

By considering mirror oscillation in a “tripod-scheme” laser-atom system, we advocate explorative studies of driven Dirac-like equations. Both analytical and numerical studies show that mirror oscillation can be used to drive an effective spin-orbit interaction and hence control the amplitude, the frequency, and the damping of the cold-atom Zitterbewegung oscillation. Our results demonstrate an interesting coupling between the mirror mechanical motion and a fundamental quantum coherent oscillation, opening up new means of matter wave manipulation.

PACS numbers: 03.75.-b, 32.80.Qk, 71.70.Ej, 37.10.Vz

I. INTRODUCTION

The jittering motion of a free relativistic electron predicted by the Dirac equation, called Zitterbewegung oscillation (ZB) [1], is a truly fundamental quantum coherence effect. Directly observing the free-electron ZB is, however, practically impossible due to its extremely high frequency and small amplitude. For this very reason, studies of ZB effect necessarily call for quantum simulations based on Dirac-like equations with (effective) spin-orbit coupling, including those involving band electrons in graphene [2], cavity electrodynamics [3], single trapped ion [4, 5], as well as ultracold atoms [6–8].

To actively explore ZB-related physics, it is necessary to go beyond passive simulations of the known ZB effect. Here we advocate to consider Dirac-like equations driven by an external field. This is feasible due to the precise controllability of laser-atom interaction. Given the current vast interest in dressed matter waves [9], this topic is also timely because it can reveal how a driven effective spin-orbit interaction may be used as a new means of matter-wave manipulation. Furthermore, as proposed below, a driven Dirac-like equation can be achieved via mirror oscillation, thus directly coupling the fascinating cold-atom ZB with the mirror mechanical motion. This interesting quantum-classical interface may lead to a novel setup of optomechanical systems [10], with spin-orbit interaction also included.

In particular, to realize a driven Dirac-like equation we propose to add oscillating mirrors [see Fig. 1(b)] to a recent cold-atom-ZB scheme [7] that involves tripod-scheme cold atoms [11–13] interacting with three laser fields. This modification induces a coupling between the mirror mechanical motion and the cold-atom matter wave, yielding a time-dependent effective spin-orbit interaction. It is shown that the amplitude of the cold-atom ZB can then be either enhanced or weakened. Such control over the ZB amplitude is also related to a dynamical realization of an effective “spin-helix” Hamiltonian [14] and the celebrated phenomenon of “coherent destruction of tunneling” (CDT) [15] in driven systems. More remarkably, the quick damping of the cold-atom ZB, which hinders experimental studies, can also be dramatically suppressed. Extending the lifetime of cold-atom ZB might be useful for finding its applications in precision measurements or sensing. It should be also stressed that although we present our findings in the cold-atom context throughout this paper, they should have direct analogs in other alternative ZB realizations mentioned above.

II. DRIVEN DIRAC-LIKE EQUATION

Consider then the interaction of a tripod-scheme cold-atom interacting with three laser fields [11, 12] [see Fig.1 (a)]. The four internal atomic levels are denoted $|n\rangle$, with $n = 0 - 3$, with the three states $|1\rangle$, $|2\rangle$, and $|3\rangle$ being degenerate magnetic sub-levels on the ground state. Each of the three laser fields has an appropriate polarization and induces a transition $|0\rangle \leftrightarrow |n\rangle$, with the Rabi frequency Ω_n , $n = 1 - 3$. In the interaction picture and under the rotating wave approximation the internal Hamiltonian is given by $H_{\text{RWA},4} = \hbar \sum_{n=1}^3 (\Omega_n |0\rangle \langle n| + \Omega_n^* |n\rangle \langle 0|)$. This Hamiltonian possesses two dark states $|D_1\rangle$, $|D_2\rangle$, with zero eigenvalue and zero overlap with the excited state $|0\rangle$. For sufficiently large Rabi frequencies Ω_n and for slow translation motion (for the system parameters associated with all our computational examples below, it can be estimated that the characteristic Rabi frequency should be around 10^7

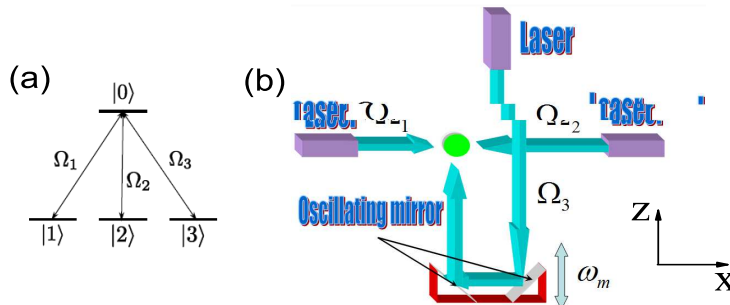


FIG. 1: (Color Online) (a) Level structure of tripod-scheme cold atoms. (b) Schematic setup involving oscillating mirrors and three laser fields interacting with cold atoms. As shown in the text, this leads to a driven Dirac-like equation.

Hz or higher), the internal state can remain in a two-dimensional dark subspace spanned by $|D_1\rangle$ and $|D_2\rangle$. In the dark state representation which can be space-dependent, the translation motion of the atom effectively experiences a non-Abelian gauge field. The total stationary Hamiltonian then becomes

$$H_S = \frac{1}{2m}(\mathbf{p} - \mathbf{A})^2 + \Phi + V, \quad (1)$$

where m is atom mass, \mathbf{p} is atom momentum, $\mathbf{A}_{ij} = i\hbar\langle D_i|\nabla D_j\rangle$ is the effective non-Abelian 2×2 potential matrix, Φ is the Born-Huang scalar potential, and V is the external potential. For convenience we assume $\Phi + V = \text{constant}$ and adopt the laser configuration studied in Ref. [13], with two laser fields counter-propagating along x , and another propagating along z , $\Omega_1 = \Omega_0 \sin(\xi)e^{-ik_l x/\sqrt{2}}$, $\Omega_2 = \Omega_0 \sin(\xi)e^{ik_l x/\sqrt{2}}$, $\Omega_3 = \Omega_0 \cos(\xi)e^{ik_l z}$, and $\cos(\xi) = \sqrt{2} - 1$, where k_l is the laser wavevector. It then suffices to consider the $x - z$ plane in Fig. 1(b) with two unit vectors \hat{e}_x and \hat{e}_z . As such, $\mathbf{p} = p_x\hat{e}_x + p_z\hat{e}_z$, and the Hamiltonian H_S becomes

$$H_S = \frac{\mathbf{p}^2}{2m} + \frac{\hbar\kappa}{m}(p_x\sigma_x + p_z\sigma_z), \quad (2)$$

where $\kappa \equiv (\sqrt{2} - 1)k_l$, and $\sigma_{x,z}$ are the standard Pauli matrices. The second term in Eq. (2) represents an effective spin-orbit coupling that resembles the Dresselhaus spin-orbit Hamiltonian (other types of spin-orbit interaction, such as a mixture of Dresselhaus and Rashba coupling, can be obtained by considering different laser configurations [7]). When the effects of the $\mathbf{p}^2/2m$ term are small as compared with the spin-orbit coupling term, the Schrödinger equation for H_S will be dominated by the second spin-orbit term in Eq. (2), which is linear in p_x or p_z . In this sense a Dirac-like equation (with two-component spinors) is obtained.

To arrive at a driven Dirac-like equation, we consider two oscillating mirrors joined together, schematically shown in Fig. 1(b). If the mirrors are moving at a velocity $v/2 = (v_d/2)\cos(\omega_d t)$ in the z direction, then effectively the Ω_3 field is moving towards the atom at a velocity v . As indicated below, such a movement is very slow as compared with the speed of light and hence relativistic Doppler effects can be safely neglected. In a moving frame where the laser source is stationary, Eq. (2) applies. We then make a Galileo transformation back to the laboratory frame, obtaining the following driven Hamiltonian

$$H_{\text{driven}} = \frac{\mathbf{p}^2}{2m} + \frac{\hbar\kappa}{m}\{[p_z - mv_d \cos(\omega_d t)]\sigma_z + p_x\sigma_x\}. \quad (3)$$

This driven Hamiltonian can be alternatively derived by considering non-Abelian geometric phases induced by the moving mirrors [16]. When the spin-orbit interaction in Eq. (3) (which is now time-dependent) accounts for the main physics, the Schrödinger equation for H_{driven} simulates a driven Dirac-like equation. In the following two driven cases will be elaborated as examples.

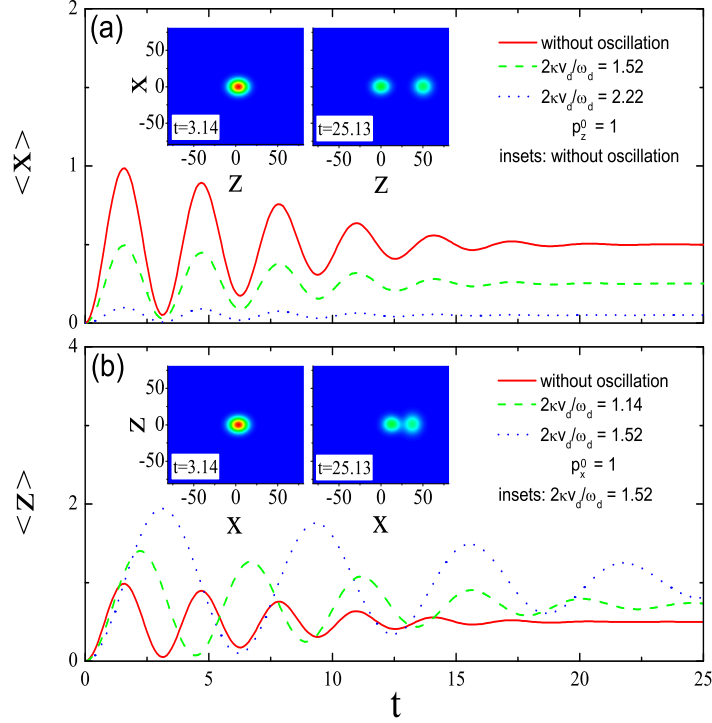


FIG. 2: (Color Online) Effects of a high-frequency mirror oscillation on cold-atom ZB. The initial momentum \mathbf{p}_0 is taken in the z direction in (a) and in the x direction in (b). Insets are the typical wavepacket profile at early and later times, with the initial variance in x and z being around 10.0. Throughout t is in units of $m/(\hbar\kappa^2)$, x and z are in units of $1/\kappa$. $\omega_d = 50$ in units of $\hbar\kappa^2/m$.

III. CONTROLLED COLD-ATOM ZITTERBEWEGUNG

Figure 2 depicts the time-dependence of the expectation value $\langle x \rangle$ or $\langle z \rangle$ of the cold atom, calculated from the evolution associated with H_{driven} . The initial state is given by $|\Psi(0)\rangle = (1/\sqrt{2}, i/\sqrt{2})^T \int d\mathbf{p} |\mathbf{p}\rangle G(\mathbf{p})$, where $\langle \mathbf{r} | \mathbf{p} \rangle \sim e^{i\mathbf{p}\cdot\mathbf{r}}$, and $G(\mathbf{p})$ is a Gaussian distribution. This initial state represents a two-component spinor in the dark state representation times a Gaussian wavepacket. The shown oscillations in $\langle x \rangle$ or $\langle z \rangle$ without mirror oscillation (solid lines) are the expected cold-atom ZB effect. But remarkably, the ZB amplitude and frequency are seen to be strongly affected by introducing the mirror oscillation. In particular, in the case of Fig. 2(a), the initial wavepacket is set to move along the z direction, ZB occurs in $\langle x \rangle$, with its amplitude tuned down extensively and with its frequency unchanged. In the case of Fig. 2(b), the initial wavepacket is set to move along the x direction, ZB occurs in $\langle z \rangle$, with its amplitude tuned up extensively and at the same time its frequency much decreased. Note that in all the shown examples the ZB frequency is much smaller than the mirror oscillation frequency ω_d .

To understand the results in Fig. 2, we adopt a perspective afforded by a standard high-frequency approximation. That is, when $1/\omega_d$ is much smaller than all other time scales, the driven dynamics can be approximately described by a static effective Hamiltonian $H_{\text{driven}}^{\text{eff}}$ via an averaging of the time-dependent term of H_{driven} , i.e., $-\hbar\kappa v_d \cos(\omega_d t) \sigma_z = H_{\text{driven}} - H_S \equiv A(t)$. To the first order of $1/\omega_d$, we obtain $H_{\text{driven}}^{\text{eff}} = (\omega_d/2\pi) \int_0^{2\pi/\omega_d} dt e^{iF(t)} H_S e^{-iF(t)}$, where $F(t) = \int_0^t dt' A(t')/\hbar$ [17]. Specifically,

$$H_{\text{driven}}^{\text{eff}} = \frac{\mathbf{p}^2}{2m} + \frac{\hbar\kappa}{m} [p_z \sigma_z + \mathcal{J}_0\left(\frac{2\kappa v_d}{\omega_d}\right) p_x \sigma_x], \quad (4)$$

where \mathcal{J}_0 is the ordinary Bessel function of order zero. Let $\theta(\tilde{\mathbf{p}})$ be the angle between the vector $\tilde{\mathbf{p}} \equiv p_x \mathcal{J}_0\left(\frac{2\kappa v_d}{\omega_d}\right) \hat{e}_x + p_z \hat{e}_z$ and the x axis, and let $\beta(\tilde{\mathbf{p}}) = \pi/4 - \theta(\tilde{\mathbf{p}})/2$. The eigenstates of $H_{\text{driven}}^{\text{eff}}$ are then found to be $|\psi^+\rangle = [\cos(\beta), \sin(\beta)]^T |\mathbf{p}\rangle$ and $|\psi^-\rangle = [\sin(\beta), -\cos(\beta)]^T |\mathbf{p}\rangle$, with their eigenvalues given by $E_{\pm}(\mathbf{p}, \tilde{\mathbf{p}}) \equiv \mathbf{p}^2/2m \pm \hbar\kappa|\tilde{\mathbf{p}}|/m$. Because each \mathbf{p} component in the initial state $|\Psi(0)\rangle$ can be expanded by the eigenstates $|\psi^{\pm}\rangle$, it can be predicted

from $H_{\text{driven}}^{\text{eff}}$ that the total state $|\Psi(t)\rangle$ at time t is given by

$$|\Psi(t)\rangle = \frac{1}{\sqrt{2}} \int d\mathbf{p} G(\mathbf{p}) e^{i\beta(\tilde{\mathbf{p}})} \times \left[e^{-\frac{iE_+(\mathbf{p}, \tilde{\mathbf{p}})t}{\hbar}} |\psi^+\rangle - ie^{-\frac{iE_-(\mathbf{p}, \tilde{\mathbf{p}})t}{\hbar}} |\psi^-\rangle \right]. \quad (5)$$

Further using $\mathbf{r} = i\hbar\nabla_{\mathbf{p}}$, one easily finds

$$\langle \mathbf{r}(t) \rangle = i\hbar \langle \Psi(t) | \nabla_{\mathbf{p}} | \Psi(t) \rangle = \mathbf{r}^0 + \mathbf{p}^0 t / m + \frac{\hbar}{2} \int d\mathbf{p} |G(\mathbf{p})|^2 [\nabla_{\mathbf{p}} \theta(\tilde{\mathbf{p}})] \{1 - \cos[\omega(\tilde{\mathbf{p}})t]\}, \quad (6)$$

where the last oscillating term represents cold-atom ZB, with the angular frequency $\omega(\tilde{\mathbf{p}}) \equiv [E_+(\mathbf{p}, \tilde{\mathbf{p}}) - E_-(\mathbf{p}, \tilde{\mathbf{p}})]/\hbar = 2\kappa|\tilde{\mathbf{p}}|/m$, \mathbf{r}^0 is the initial expectation value of \mathbf{r} , and \mathbf{p}^0 is the initial momentum of the Gaussian wavepacket.

We now come back to the results in Fig. 2. In the case of Fig. 2(a), $p_x \approx 0$, $\mathbf{p} \approx p_z \hat{e}_z$, then $\omega(\tilde{\mathbf{p}}) \approx \omega(\mathbf{p})$ and

$$\nabla_{\mathbf{p}} \theta(\tilde{\mathbf{p}}) \approx -\frac{\mathcal{J}_0\left(\frac{2\kappa v_d}{\omega_d}\right)}{p_z} \hat{e}_x. \quad (7)$$

Substituting these two relations into Eq. (6), one directly obtains that ZB is along x , its amplitude is proportional to the factor $\mathcal{J}_0\left(\frac{2\kappa v_d}{\omega_d}\right)$, and its frequency is independent of ω_d . Quantitatively, for the two shown examples with $2\kappa v_d/\omega_d = 1.52$ or 2.22 in Fig. 2(a), the ZB amplitude should decrease by a factor of 2.0 or 10.0 as compared with that without mirror oscillation ($v_d = 0$), in excellent agreement with the numerics. Likewise, in the case of Fig. 2(b), $p_z \approx 0$, $\mathbf{p} \approx p_x \hat{e}_x$, leading to $\omega(\tilde{\mathbf{p}}) \approx \mathcal{J}_0\left(\frac{2\kappa v_d}{\omega_d}\right)\omega(\mathbf{p})$ and

$$\nabla_{\mathbf{p}} \theta(\tilde{\mathbf{p}}) \approx \frac{1}{p_x \mathcal{J}_0\left(\frac{2\kappa v_d}{\omega_d}\right)} \hat{e}_z. \quad (8)$$

Equation (6) then predicts that ZB is now along z , its amplitude is proportional to the factor $1/\mathcal{J}_0\left(\frac{2\kappa v_d}{\omega_d}\right)$, and the ZB frequency is proportional to $\mathcal{J}_0\left(\frac{2\kappa v_d}{\omega_d}\right)$. For the two examples with $2\kappa v_d/\omega_d = 1.14$ or 1.52 in Fig. 2(b), the ZB amplitude should be enhanced by a factor of 1.41 or 2.0 as compared with that without mirror oscillation, and the associated ZB frequency should be decreased by a factor 0.7 or 0.5. This is again in agreement with our direct numerical experiments. Note that if we have $\mathcal{J}_0\left(\frac{2\kappa v_d}{\omega_d}\right) = 0$, i.e., exactly on a CDT point [15] where the transition between the two dark states is totally suppressed by the driving, then in the case of Fig. 2(a), the ZB amplitude is zero, and in the case of Fig. 2(b), the ZB frequency is zero. So in either case the ZB effect disappears on a CDT point. Interestingly, this is also a situation where $H_{\text{driven}}^{\text{eff}}$ takes a spin-helix form [14], which now possesses an SU(2) symmetry. Such a dynamical realization of a spin-helix Hamiltonian constitutes an intriguing consequence of the coupling between the mechanical mirror oscillation and the effective spin-orbit interaction.

Results in Fig. 2 also indicate that in general cold-atom ZB in a two-dimensional geometry suffers from quick damping [18], thus setting limitations to its potential application. This ZB damping can have two different, but related, interpretations. First, Eq. (6) involves an integral over a continuous distribution of the ZB frequency $\omega(\tilde{\mathbf{p}})$. As time evolves, oscillations associated with different \mathbf{p} comprising the initial wavepacket will necessarily dephase. This makes it clear that the lifetime of the ZB is inversely proportional to the momentum spread in the initial wavepacket [7]. The second picture is more enlightening. Note that the oscillating term in Eq. (6) is due to the quantum interference between the $|\psi^+\rangle$ and $|\psi^-\rangle$ branches in Eq. (5). Because these two terms have different group velocities $\nabla_{\mathbf{p}} E_{\pm}(\mathbf{p}, \tilde{\mathbf{p}}) = \mathbf{p}/m \pm \hbar\kappa\nabla_{\mathbf{p}}|\tilde{\mathbf{p}}|/m$, the wavepacket on the $|\psi^+\rangle$ branch will move away from that on the $|\psi^-\rangle$ branch (see insets in Fig. 2). As a consequence the overlap of the two wavepackets decreases with time, their quantum interference decays, and hence ZB damps. The CDT condition $\mathcal{J}_0\left(\frac{2\kappa v_d}{\omega_d}\right) = 0$ may eliminate this group velocity difference, but as mentioned above, it also kills ZB in the beginning.

To dynamically suppress the ZB damping of a two-dimensional cold-atom wavepacket, we next consider a different regime of ω_d . Suppose the initial wavepacket has an average momentum p_x^0 (p_z^0) along the x (z) direction, with $p_x^0 \gg p_z^0$. We let ω_d satisfy the following ‘‘resonance’’ condition: $p_x^0 \approx m\omega_d/2\kappa$, with $\omega_d \gg \kappa p_z^0/m, \kappa v_d$. In this regime, ω_d matches the precession frequency of the effective spin around p_x^0 . However, in a rotating frame, where the spinor wavefunction $(a', b')^T$ is related to the wavefunction $(a, b)^T$ in a non-rotating frame by

$$\begin{pmatrix} a' \\ b' \end{pmatrix} = \frac{a+b}{2} \begin{pmatrix} 1 \\ 1 \end{pmatrix} e^{\frac{i\omega_d t}{2}} + \frac{a-b}{2} \begin{pmatrix} 1 \\ -1 \end{pmatrix} e^{-\frac{i\omega_d t}{2}}, \quad (9)$$

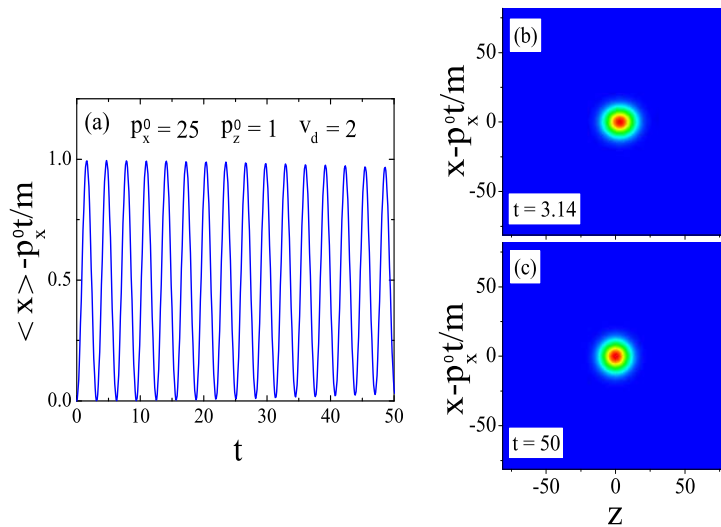


FIG. 3: (Color Online) (a) Suppression of ZB damping by mirror oscillation in an on-resonance regime. The initial momentum spread and ω_d are the same as in Fig. 2. Panels (b) and (c) demonstrate that the wavepacket does not split despite the ZB.

ω_d still dominates over all other frequencies. One can then apply again the above-introduced high-frequency approximation and obtain the following effective Hamiltonian in the rotating frame (for $v_d \kappa / \omega_d \ll 1$)

$$H_{\text{reso}}^{\text{eff}} = \frac{\mathbf{p}^2}{2m} + \frac{\hbar \kappa}{m} \left[\frac{m v_d}{2} \sigma_z + \left(p_x - \frac{m \omega_d}{2 \kappa} \right) \sigma_x \right]. \quad (10)$$

Eigenvalues of this effective on-resonance Hamiltonian are given by $E_{\pm}^{\text{reso}}(\mathbf{p}) = \mathbf{p}^2/2m \pm (\hbar \kappa/m) \left[(m v_d/2)^2 + (p_x - m \omega_d/2 \kappa)^2 \right]^{1/2} \approx \mathbf{p}^2/2m \pm \hbar \kappa v_d/2$, where we have used the resonance condition $p_x^0 \approx m \omega_d/2 \kappa$ and the assumption that the p_x of a wavepacket is strongly peaked at p_x^0 . Same as in our early consideration, the beating frequency between the two eigenvalue branches, i.e., $\omega^{\text{reso}}(\mathbf{p}) \equiv E_+^{\text{reso}}(\mathbf{p})/\hbar - E_-^{\text{reso}}(\mathbf{p})/\hbar$, gives rise to the new ZB frequency $\omega^{\text{reso}}(\mathbf{p}) \approx \kappa v_d$. This indicates that now the ZB frequency is totally determined by the velocity amplitude v_d of the mirror oscillation, thus entirely converting a mechanical property of the mirror to that of a fundamental quantum coherence phenomenon. Further, it is easy to find that $\langle \mathbf{r} \rangle$ here can still be given by Eq. (6), but with $\tilde{\mathbf{p}} = (p_x - m v_d/2 \kappa) \hat{e}_x + (m v_d/2) \hat{e}_z \approx (m v_d/2) \hat{e}_z$. Further evaluating $\nabla_{\mathbf{p}} \theta(\tilde{\mathbf{p}})$ in Eq. (6), one finds that the ZB here should be along the x direction.

Significantly, the group velocities for both the eigenvalue branches $E_{\pm}^{\text{reso}}(\mathbf{p})$ now become the same, i.e., $\nabla_{\mathbf{p}} E_{\pm}^{\text{reso}}(\mathbf{p}) \approx \frac{\mathbf{p}}{m}$. Hence, an initial wavepacket undergoing ZB will not split into two parts. According to our early explanation of the ZB damping seen in Fig. 2, such suppression of wavepacket splitting should suppress the damping of ZB. Numerical results in Fig. 3 directly using H_{driven} confirm our predictions based on $H_{\text{reso}}^{\text{eff}}$. In particular, the initial state used in Fig. 3 has the same momentum spread as in Fig. 2, and the mirror oscillation is now under the resonance condition $p_x^0 \approx m \omega_d/2 \kappa$. It is seen from Fig. 3 that the wavepacket does not split despite the ZB. For a similar ZB frequency as in Fig. 2(a), the ZB damping can be hardly seen in Fig. 3, even after doubling the time scale. It can be estimated that via the mirror oscillation the ZB lifetime here is increased by more than one order of magnitude.

IV. CONCLUSION

To conclude, by considering mirror oscillation in a laser-atom system, we have proposed to explore time-dependent Dirac-like equations via driving an effective spin-orbit interaction. Using cold-atom ZB as a case study, we have shown how mirror oscillation can be used to control the amplitude, the frequency, and the lifetime of ZB in a two-dimensional geometry. For $m \sim 10^{-25}$ Kg, $\kappa \sim 10^6$ m $^{-1}$, $|\mathbf{p}| \sim 1 - 10 \hbar \kappa$, we find $\omega_m \sim 10^4$ Hz, falling in the range of the mirror oscillation frequency in current optomechanical systems [10]. This also suggests that the peak velocity of the mirror is of the order of $10^{-3} - 10^{-2}$ ms $^{-1}$. In addition to opening up a new means of matter-wave manipulation, our theoretical work should greatly motivate experimental efforts in realizing and exploring cold-atom Zitterbewegung.

ACKNOWLEDGMENTS: This work was supported by the CQT WBS grant No. R-710-000-008-271 (ZQ and CH), and by the “YIA” fund (WBS grant No.: R-144-000-195-101) (JG) of the National University of Singapore.

-
- [1] E. Schrödinger *et al.*, *Physikmath. Kl.* **24**, 418 (1930).
 - [2] K. S. Novoselov *et al.*, *Science* **306**, 666 (2004).
 - [3] J. Larson and S. Levin, *Phys. Rev. Lett.* **103**, 013602 (2009).
 - [4] L. Lamata, J. León, T. Schätz, and E. Solano, *Phys. Rev. Lett.* **98**, 253005 (2007).
 - [5] R. Gerritsma, G. Kirchmair, F. Zähringer, E. Solano, R. Blatt, and C.F. Roos, *Nature* **463**, 68 (2010).
 - [6] G. Juzeliunas *et al.*, *Phys. Rev. A* **77**, 011802(R)(2008).
 - [7] J. Y. Vaishnav and C. W. Clark, *Phys. Rev. Lett.* **100**, 153002 (2008).
 - [8] M. Merkl *et al.*, *EPL* **83**, 54002 (2008).
 - [9] For example, A. Zenesini *et al.*, *Phys. Rev. Lett.* **102**, 100403 (2009); A. Eckardt and M. Holthaus, *Phys. Rev. Lett.* **101**, 245302 (2008).
 - [10] S. Gröblacher *et al.*, *Nature Phys.* **5**, 485 (2009); P. F. Herskind *et al.*, *Nature Phys.* **5**, 494 (2009); F. Brennecke *et al.*, *Science* **322**, 235 (2008); F. Brennecke *et al.*, *Nature* **450**, 268 (2007); K. Hammerer *et al.*, *Phys. Rev. Lett.* **103**, 063005 (2009).
 - [11] R. G. Unanyan, B. W. Shore, and K. Bergmann, *Phys. Rev. A* **59**, 2910 (1999).
 - [12] J. Ruseckas *et al.*, *Phys. Rev. Lett.* **95**, 010404 (2005).
 - [13] G. Juzeliunas *et al.*, *Phys. Rev. Lett.* **100**, 200405 (2008).
 - [14] B. A. Bernevig, J. Orenstein, and S. C. Zhang, *Phys. Rev. Lett.* **97**, 236601 (2006).
 - [15] F. Grossmann, T. Dittrich, P. Jung, and P. Hänggi, *Phys. Rev. Lett.* **67**, 516 (1991).
 - [16] Q. Zhang, J. B. Gong, and C. H. Oh, *Phys. Rev. A* **79**, 043632 (2009).
 - [17] S. Kohler, J. Lehmann, and P. Hänggi, *Phys. Rep.* **406**, 379 (2005); see pp. 401-402.
 - [18] As seen in Ref. [8], if the system can be confined to quasi-one-dimensional geometries (hence the vector potential \mathbf{A} becomes Abelian), then the damping of ZB is less severe.